Standard and non-standard neutrino oscillations

J. W. F. Valle

Instituto de Física Corpuscular
C.S.I.C./Universitat de València
Edificio Institutos de Paterna, Apt 22085
E–46071 València, Spain

Abstract. I describe recent determination of neutrino oscillation parameters from solar and atmospheric data, comparing the results of different analyses. Non-oscillation phenomena such as neutrinoless double beta decay in addition to probing the absolute scale of neutrino mass, may also reveal its Majorana nature. I also discuss non-oscillation solutions to the solar neutrino problem in terms of spin-flavor precession and non-standard neutrino interactions, which will be crucially tested at KamLAND.

1. SOLAR NEUTRINOS

Solar neutrinos have now been detected with the geochemical method via the $\nu_e + {}^{37}\mathrm{Cl} \to {}^{37}\mathrm{Ar} + e^-$ reaction at Homestake, and via the $\nu_e + {}^{71}\mathrm{Ga} \to {}^{71}\mathrm{Ge} + e^-$ reaction at the Gallex, Sage and GNO experiments, as well as directly with Cherenkov techniques using $\nu_e e$ scattering on water at Super-K, and heavy water at SNO [1]. The latter have given a robust confirmation that the number of solar neutrinos detected in underground experiments is less than expected from theories of energy generation in the sun. Altogether these experiments provide a solid evidence for solar neutrino conversions and, as a result, imply that an extension of the Standard Model of particle physics in the lepton sector is needed.

Although not yet unique, the most popular explanation of solar neutrino experiments is provided by the neutrino oscillations hypothesis. Present data indicate that the mixing angle is large [2], the best description being given by the LMA MSW-type [3] solution, already hinted previously from the flat Super-K recoil electron spectra [4, 5]. The absence of a clear hint for day-night or seasonal variation in the solar neutrino signal places important restrictions on neutrino parameters.

In ref. [2] the solar neutrino data, including the latest 1496–day data and the SNO neutral current (NC) result have been analysed in the general framework of mixed active-sterile neutrino oscillations, where the electron neutrino produced in the sun converts to ν_x (a combination of ν_μ and ν_τ) and a sterile neutrino ν_s : $\nu_e \to \sqrt{1-\eta_s}\,\nu_x + \sqrt{\eta_s}\,\nu_s$. The setting for such scenarios are four-neutrino mass schemes [6] which try to accommodate the solar and atmospheric mass-splittings with the hint for short baseline oscillations from LSND [7] indicating a large Δm^2. The parameter η_s with $0 \leq \eta_s \leq 1$ describes the fraction of sterile neutrinos taking part in the solar oscillations.

In Fig. 1 we display the regions of solar neutrino oscillation parameters for 3 d.o.f. with respect to the global minimum, for the standard case of active oscillations, $\eta_s = 0$, as well as for $\eta_s = 0.2$ and $\eta_s = 0.5$. The first thing to notice is the impact of the SNO NC, spectral, and day/night data in improving the determination of the oscillation parameters: the shaded regions after their inclusion are much smaller than the hollow regions delimited by the corresponding $\mathrm{SNO}_{\mathrm{CC}}^{\mathrm{rate}}$ confidence contours. Especially important is the full $\mathrm{SNO}_{\mathrm{CC,NC}}^{\mathrm{SP,DN}}$ information in closing the LMA region from above: values of $\Delta m^2_{\mathrm{SOL}} > 10^{-3}$ eV^2 appear only at 3σ. Previously solar data on their own could not close the LMA region, only the inclusion of reactor data [8] probed the upper part of the LMA region [5]. Furthermore, the complete $\mathrm{SNO}_{\mathrm{CC,NC}}^{\mathrm{SP,DN}}$ information is important for excluding `maximal` solar mixing in the LMA region. At 3σ we find (1 d.o.f.):

$$\mathrm{LMA}: \quad 0.26 \leq \tan^2\theta_{\mathrm{SOL}} \leq 0.85\,. \tag{1}$$

showing that in the LMA region $\tan^2\theta_{\mathrm{SOL}}$ is significantly below maximal.

As discussed in ref. [2] all groups find that the best fit lies in the LMA region, although there are quantitative differences even for this preferred solution, with the GOF of the best-fit LMA solution, ranging from 53% to 97%.

Generally speaking, one expects the differences in the statistical treatment of the data to have little impact close to the global best fit point, located in the LMA region. These differences typically become more visible as one departs from the best fit region towards more disfavored solutions. Aware of this, ref. [2] took special care to details such as the dependence of the theoretical errors on the oscillation parameters, which enter in the covariance matrix characterizing the Super-K and SNO electron recoil spectra. This way results reliable in the full oscillation parameter space were obtained.

Despite differences in the various solar neutrino data analyzes there is relatively good agreement on the best fit LMA active oscillation parameters: the obtained best fit values for $\tan^2\theta_{\mathrm{SOL}}$ are in the range $0.34-0.47$ and for $\Delta m^2_{\mathrm{SOL}}$ they lie in the interval $(5.0-7.9)\times 10^{-5}$ eV^2. There is also good agreement on the allowed ranges of the oscillation parameters. There is remarkable agreement on the rejection of the LOW solution with respect to LMA with a $\Delta\chi^2_{\mathrm{LOW,active}} \approx 10$. The result for the vacuum solution in [2] $\Delta\chi^2_{\mathrm{VAC,active}} = 8.9$ is in good agreement with the values obtained by the Super-K collaboration, as well as Bahcall et al, de Holanda & Smirnov and Fogli et al, whereas Bandyopadhyay et al, Barger et al and Creminelli etal obtain higher values. Our result for the SMA solution of $\Delta\chi^2_{\mathrm{SMA,active}} = 23.2$ is in good agreement with the values obtained in Bahcall et al, Creminelli et al and Fogli et al; while Bandyopadhyay et al and de Holanda & Smirnov, and especially Barger et al obtain higher values.

All in all, taking into account the vast input data, variations in the analysis (such as the construction of the χ^2 function or the treatment of errors and their correlations) and the complexity of the codes involved it seems encouraging that there is reasonable agreement amongst different analyzes. Scrutinizing the origin of the differences which are found is not an easy task. Typically the results of a given analysis away from the best fit region serve as an indicator of its quality.

Note that in order to compare the allowed regions in Fig. 1 with others, one must note that our C.L. regions correspond to the 3 d.o.f. corresponding to $\tan^2\theta_{\mathrm{SOL}}$, $\Delta m^2_{\mathrm{SOL}}$ and η_s. Therefore at a given C.L. our regions are larger than the usual regions for 2 d.o.f., because we also constrain the parameter η_s. Our global best fit point occurs

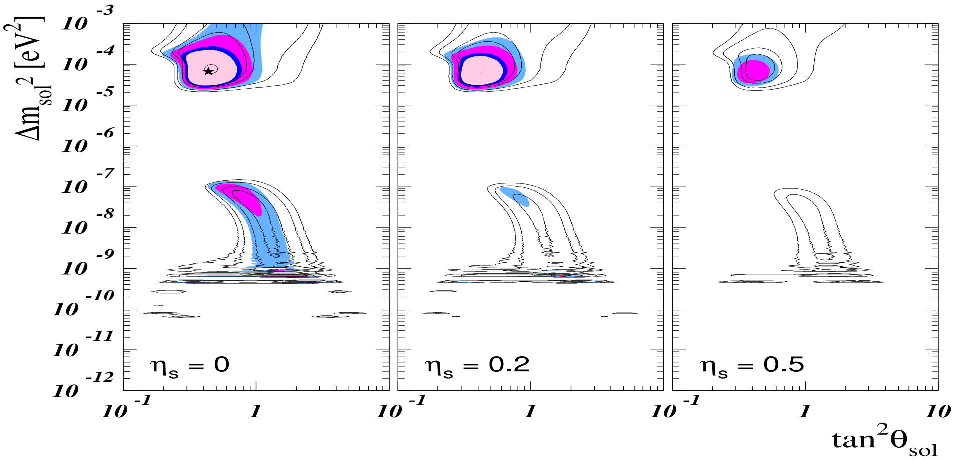

Figure 1. Allowed $\tan^2\theta_{\rm SOL}$ and $\Delta m^2_{\rm SOL}$ regions for $\eta_s = 0$ (active oscillations), $\eta_s = 0.2$ and $\eta_s = 0.5$. The lines and shaded regions correspond to the $\text{SNO}^{\text{rate}}_{\text{CC}}$ and $\text{SNO}^{\text{SP,DN}}_{\text{CC,NC}}$ analyses, respectively, as defined in Ref. [2]. The 90%, 95%, 99% C.L. and 3σ contours are for 3 d.o.f..

for active oscillations with

$$\tan^2\theta_{\rm SOL} = 0.46\,, \quad \Delta m^2_{\rm SOL} = 6.6\times 10^{-5}\ {\rm eV}^2 \tag{2}$$

A concise way to illustrate the above results is displayed in Fig. 2. We give the profiles of $\Delta\chi^2_{\rm SOL}$ as a function of $\Delta m^2_{\rm SOL}$ (left) as well as $\tan^2\theta_{\rm SOL}$ (right), by minimizing with respect to the undisplayed oscillation parameters, for the fixed values of $\eta_s = 0$, 0.5, 1. By comparing top and bottom panels one can clearly see the impact of1 the

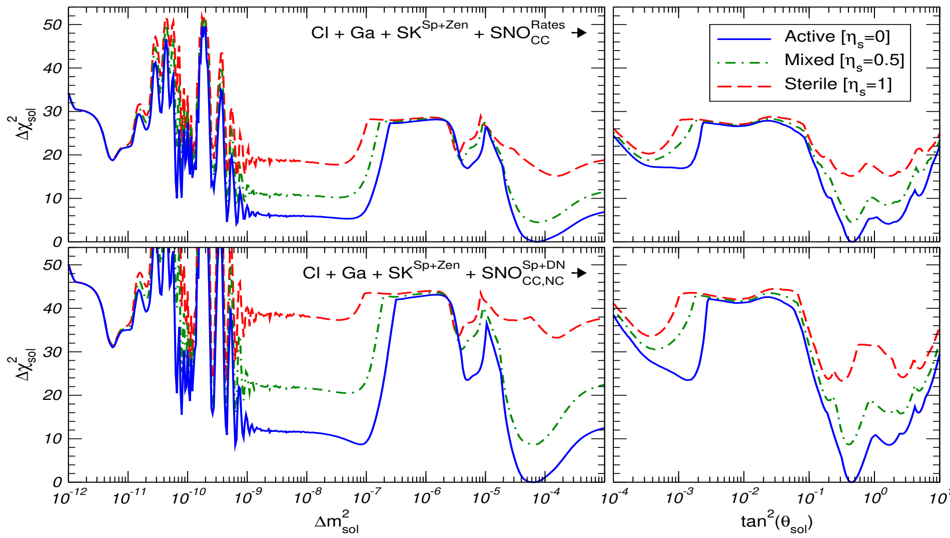

Figure 2. $\Delta\chi^2_{\rm SOL}$ as a function of $\Delta m^2_{\rm SOL}$ and $\tan^2\theta_{\rm SOL}$, for pure active ($\eta_s = 0$), pure sterile ($\eta_s = 1$) and mixed neutrino oscillations ($\eta_s = 0.5$). Upper and lower panels correspond to the $\text{SNO}^{\text{rate}}_{\text{CC}}$ and $\text{SNO}^{\text{SP,DN}}_{\text{CC,NC}}$ samples defined in Ref. [2].

full $\text{SNO}^{\text{SP,DN}}_{\text{CC,NC}}$ sample in leading to the relative worsening of all non-LMA solutions with respect to the preferred active LMA solution. One sees also how the preferred LMA status survives in the presence of a small sterile admixture characterized by η_s (also seen in Figs. 1 and 3). Increasing η_s leads to a deterioration of all oscillation solutions.

It is also instructive to display the profile of $\Delta\chi^2_{\text{SOL}}$ as a function of $0 \le \eta_s \le 1$, irrespective of the detailed values of the solar neutrino oscillation parameters Δm^2_{SOL} and θ_{SOL}, as shown in Fig. 3. One can see that there is a crossing between the LMA

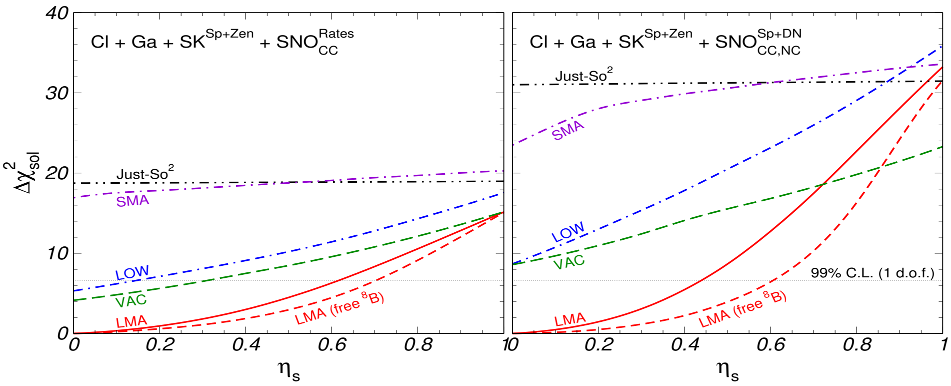

Figure 3. $\Delta\chi^2_{\text{SOL}}$ displayed as a function of η_s with respect to favored active LMA solution, for the $\text{SNO}^{\text{rate}}_{\text{CC}}$ (left panel) and the $\text{SNO}^{\text{SP,DN}}_{\text{CC,NC}}$ (right panel) analysis, as defined in Ref. [2].

and quasi–vacuum–oscillations (QVO) solutions. This implies that the best pure–sterile description lies in the QVO regime. However, in the global analysis pure sterile oscillations with $\eta_s = 1$ are highly disfavored. We find a χ^2-difference between pure active and sterile of $\Delta\chi^2_{\text{s}-\text{a}} = 32.9$ if we restrict to the LMA solution, or $\Delta\chi^2_{\text{s}-\text{a}} = 22.9$ if we allow also for QVO. For 3 d.o.f. the $\Delta\chi^2_{\text{s}-\text{a}} = 22.9$ implies that pure sterile oscillations are ruled out at 99.996% C.L. compared to the active case. From the figure we obtain the bound

$$\text{solar data}: \quad \eta_{\text{s}} \le 0.44\,(\text{boron}-\text{fixed}), \quad \eta_{\text{s}} \le 0.61\,.(\text{boron}-\text{free}).\tag{3}$$

at 99% C.L. for 1 d.o.f.. A complete table of best fit values of Δm^2_{SOL} and θ_{SOL} with the corresponding χ^2_{SOL} and GOF values for pure active, pure sterile, and mixed neutrino oscillations is given in [2], both for the $\text{SNO}^{\text{rate}}_{\text{CC}}$ $(48-2$ d.o.f.) and the $\text{SNO}^{\text{SP,DN}}_{\text{CC,NC}}$ analysis $(81-2$ d.o.f.).

2. ATMOSPHERIC NEUTRINOS

Here I summarize the analysis of atmospheric data given in Ref. [2], in a generalized oscillation scheme in which a light sterile neutrino takes part in the oscillations, under the approximation $\Delta m^2_{\text{SOL}} \ll \Delta m^2_{\text{ATM}}$ (for earlier pure active descriptions see, for example, ref. [9] and references therein). In order to comply with the strong constraints from reactor experiments [8] we completely decouple the electron neutrino from atmospheric oscillations. In contrast with the case of solar oscillations, the constraints on the ν_μ–content in atmospheric oscillations are not so stringent. Thus the description of atmospheric neutrino oscillations in this general framework requires `two new parameters` besides the standard 2-neutrino oscillation parameters θ_{ATM} and

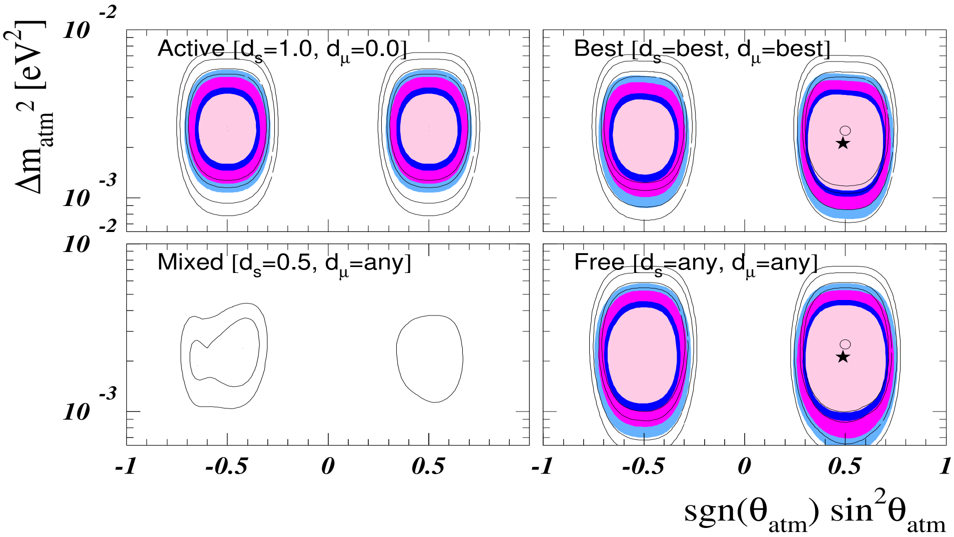

Figure 4. Allowed regions of $\sin^2\theta_{\rm ATM}$ and $\Delta m^2_{\rm ATM}$ at 90%, 95%, 99% and 3σ for 4 d.o.f. and different assumptions on the parameters d_s and d_μ, from [2]. The lines (shaded regions) correspond to 1289 (1489) days of Super-K data.

$\Delta m^2_{\rm ATM}$. We will use the parameters d_μ and d_s already introduced in Ref. [10], and defined in such a way that $1-d_\mu$ $(1-d_s)$ corresponds to the fraction of ν_μ (ν_s) participating in oscillations with $\Delta m^2_{\rm ATM}$. Hence, pure active atmospheric oscillations with $\Delta m^2_{\rm ATM}$ are recovered when $d_\mu=0$ and $d_s=1$. In four-neutrino models there is a mass-scheme-dependent relationship between d_s and the solar parameter η_s. For details see Ref. [10].

To get a feeling on the physical meaning of these two parameters, note that for $d_\mu=0$ we obtain that the ν_μ oscillates with $\Delta m^2_{\rm ATM}$ to a linear combination of ν_τ and ν_s given as $\nu_\mu \to \sqrt{d_s}\,\nu_\tau + \sqrt{1-d_s}\,\nu_s$.

Our global best fit point occurs at

$$\sin^2\theta_{\rm ATM} = 0.49\,, \quad \Delta m^2_{\rm ATM} = 2.1\times 10^{-3}\ {\rm eV}^2 \tag{4}$$

and has $d_s=0.92$, $d_\mu=0.04$. We see that atmospheric data prefers a small sterile neutrino admixture. However, this effect is not statistically significant, since the pure active case $(d_s=1, d_\mu=0)$ also gives an excellent fit: the difference in χ^2 with respect to the best fit point is only $\Delta\chi^2_{\rm act-best}=3.3$. For the pure active best fit point we obtain,

$$\sin^2\theta_{\rm ATM} = 0.5\,,\ \Delta m^2_{\rm ATM} = 2.5\times 10^{-3}\ {\rm eV}^2 \tag{5}$$

with the 3σ ranges (1 d.o.f.)

$$0.3 \le \sin^2\theta_{\rm ATM} \le 0.7 \tag{6}$$

$$1.2\times 10^{-3}\ {\rm eV}^2 \le \Delta{\rm m}^2_{\rm ATM} \le 4.8\times 10^{-3}\ {\rm eV}^2\,. \tag{7}$$

The determination of the parameters $\theta_{\rm ATM}$ and $\Delta m^2_{\rm ATM}$ is summarized in Figs. 4 and 5. Note that Fig. 5 considers several cases: arbitrary d_s and d_μ, best–fit d_s and d_μ, and pure active and mixed active–sterile neutrino oscillations, as indicated.

At a given C.L. we cut the $\chi^2_{\rm ATM}$ at a $\Delta\chi^2$ determined by 4 d.o.f. to obtain 4-dimensional volumes in the parameter space of $(\theta_{\rm ATM}, \Delta m^2_{\rm ATM}, d_\mu, d_s)$. In the upper panels we show sections of these volumes at values of $d_s = 1$ and $d_\mu = 0$ corresponding to the pure active case (left) and the best fit point (right). Again we observe that moving from pure active to the best fit does not change the fit significantly. In the lower right panel we project away both d_μ and d_s, whereas in the lower left panel we fix $d_s = 0.5$ and eliminate only d_μ. Comparing the regions resulting from 1489 days Super-K data (shaded regions) with the one from the 1289 days Super-K sample (hollow regions) we note that the new data leads to a slightly better determination of $\theta_{\rm ATM}$ and $\Delta m^2_{\rm ATM}$. However, more importantly, from the lower left panel we see, that the new data shows a much stronger rejection against a sterile admixture: for $d_s = 0.5$ no allowed region appears at 3σ for 4 d.o.f..

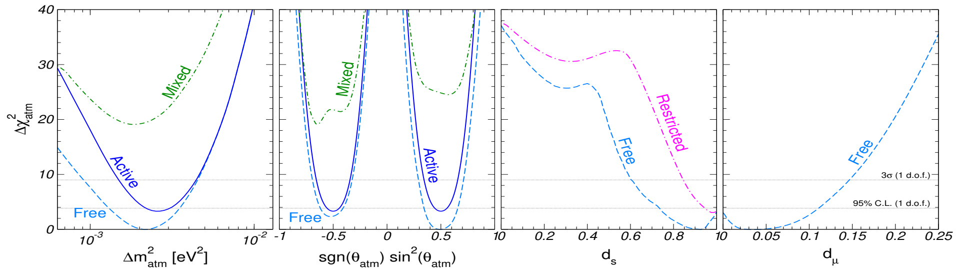

Figure 5. $\Delta\chi^2_{\rm ATM}$ as a function of $\Delta m^2_{\rm ATM}$, $\sin^2\theta_{\rm ATM}$, d_s and d_μ. In each panel the undisplayed parameters are integrated out. The "Mixed" and "Restricted" cases correspond to $d_s = 0.5$ and $d_\mu = 0$, respectively [2].

3. NEUTRINO PARAMETERS

The basic structure of the neutrino sector required to account for present solar and atmospheric data has been developed in the early eighties, motivated mainly by theory [11, 12, 13, 14]. In a gauge theory of the weak interaction the `simplest` lepton mixing matrix is characterized by 3 angles and 3 CP violating phases [15]:

- the solar angle θ_{12}
- the atmospheric angle θ_{23}
- the reactor angle θ_{13}
- one Kobayashi-Maskawa-like CP phase
- 2 extra (Majorana-type) CP phases

The structure of leptonic weak interactions is more complex in theories containing $SU(2) \otimes U(1)$ singlet leptons, especially if, for some symmetry reason, they happen to be light. In such case the charged current mixing matrix is rectangular and the neutral current is non-trivial, with yet new angles and phases present (see [15] for a detailed discussion and parametrization).

As seen above, current solar and atmospheric data fit very well with oscillations among the three active neutrinos, provided that θ_{12} is large as seen in Eq. (2), but non-maximal, given in Eq. (1), while θ_{23} must be nearly maximal, from Eq. (5). As mentioned, θ_{13} must be rather small [5]. Note from Eqs. (2) and (5) that $\Delta m^2_{\rm ATM} \gg \Delta m^2_{\rm SOL}$. Depending on the sign of Δm^2_{32} there are two possible neutrino mass schemes: normal and inverse-hierarchical neutrino masses.

If solar and atmospheric data are combined with short baseline data including the LSND hint, then one needs, in the framework of the oscillation hypothesis, the existence of a light sterile neutrino [6] taking part in the oscillations [10].

With the latest data one finds that, even though 4-neutrino models can not be ruled out as such, the resulting global fit of all current oscillation data is extremely poor [16].

It should be clear that neutrino oscillations are sensitive only to mass splittings, not to the absolute scale of neutrino mass, nor to whether neutrinos are Dirac or Majorana particles. The main process relevant to decide this fundamental issue is $\beta\beta_{0\nu}$ decay [17]. The `black-box theorem` states that, in a "natural" gauge theory, irrespective of how $\beta\beta_{0\nu}$ is engendered, it implies a Majorana neutrino mass, and vice-versa, as illustrated by Fig. 6. One may quantify the implications

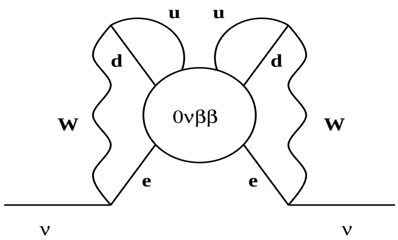

Figure 6. The black-box $\beta\beta_{0\nu}$ argument [18].

of the black-box argument once a particular model is specified. The strength of neutrino-exchange-induced $\beta\beta_{0\nu}$ is characterized by an "effective" neutrino mass parameter M_{ee} which takes into account possible cancellations among individual neutrino amplitudes [19, 20]. As seen in Fig. 7 this is directly correlated [21] with the neutrino mass scales probed in tritium beta decays [22] and cosmology [23]. It is therefore important to probe $\beta\beta_{0\nu}$ in a more sensitive experiment, such as GENIUS [24]. Moreover $\Delta L = 2$ processes, such as $\beta\beta_{0\nu}$ decay, are sensitive to the "Majorana-

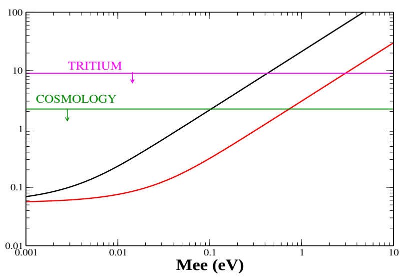

Figure 7. $\beta\beta_{0\nu}$ and the scale of neutrino mass.

type" phases [15, 25] which drop out from ordinary ($\Delta L = 0$) neutrino oscillations. Given present uncertainties these phases can not be reliably extracted from $\beta\beta_{0\nu}$ alone. Direct tests of leptonic ("Dirac") CP violation in oscillation experiments, such as neutrino factories, will be a tough challenge, due to the hierarchical neutrino mass splittings and the smallness of θ_{13} indicated by reactors (the CP violation disappears as two neutrinos become degenerate [26] and as $\theta_{13} \to 0$ [8]). Fortunately the LMA solution helps, so with good luck, neutrino factories may probe leptonic CP violating effects, through the measurement of CP asymmetries.

4. NON-STANDARD NEUTRINOS

Non-standard neutrinos interactions (NSI) are expected in most neutrino mass models [15, 27] and can be of two types: flavour-changing (FC) and non-universal (NU). They may arise from a nontrivial structure of CC and NC weak interactions characterized a non-unitary lepton mixing matrix and a correspondingly non-trivial NC matrix [15]. Such gauge-induced NSI may lead to flavor and CP violation, even with degenerate massless neutrinos [28]. In radiative models of neutrino mass [29] and supersymmetric models with broken R parity [30, 31] FC-NSI can also be Yukawa-induced, from the exchange of spinless bosons. In supersymmetric unified models, they may be calculable as renormalization effects [32].

4.1. NSI solutions to the solar neutrino problem

At the moment one can not yet pin down the exact profile of the ν_e survival probability and, as a result, the underlying mechanism of solar neutrino conversion remains unknown. Alternatives to oscillations have been suggested since the eighties, including non-standard neutrino matter interactions (NSI) [33] and spin-flavor precession (SFP) [34, 35]. The former may be represented as effective dimension-6 terms of the type εG_F, as illustrated in Fig. 8, where ε specifies their sub-weak strength.

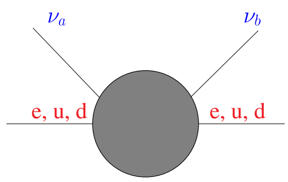

Figure 8. Effective NSI operator.

Analyses of solar neutrino data in terms of NSI [36] and SFP [37, 38, 39] have been given recently. SFP solutions exist both in the resonant (RSFP) [39] and non-resonant regimes (NRSFP) [38]. The NSI solar neutrino energy spectrum is undistorted, in agreement with data. On the other hand Fig. 9 shows the predicted modification of the solar neutrino spectra for the "best" LMA solution, and for the "best" SFP solutions [37], from latest solar data. Clearly the spectra in the high energy region are nearly undistorted in all 3 cases, in agreement with observations.

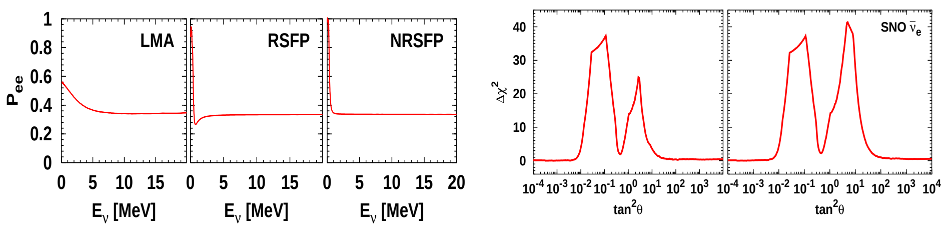

Figure 9. Best LMA and SFP ν_e survival probabilities (left) and $\Delta\chi^2_{\rm SOL}$ versus $\tan^2\theta_{\rm SOL}$, for RSFP, LMA (central minima) and NRSFP solutions, from two different analyses described in Ref. [37].

Although LMA oscillations are clearly favored over other oscillation solutions [2], present solar neutrino data can be equally well-described by SFP

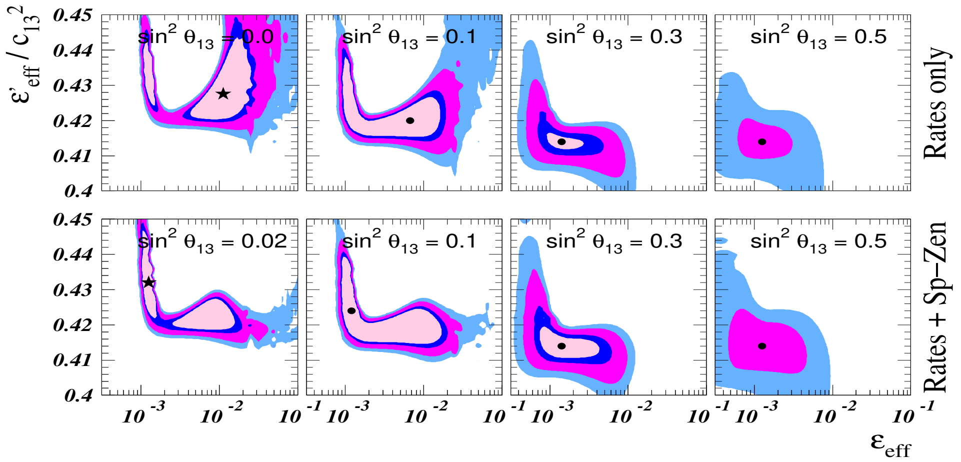

Figure 10. Parameters of NSI solution to the solar neutrino anomaly, from [36].

`and NSI solutions`. Fig. 9 shows how this happens in the SFP-oscillation case, the resulting parameter regions is given in [37]. Apart from the fact that the two SFP solutions lie slightly lower than the LMA minimum, the 3 solutions are statistically equivalent. Ways to distinguish LMA from the NRSFP solution and the simplest RSFP solution at Borexino have been considered in Refs. [37, 40]. On the other hand, if the LMA solution is finally confirmed by KamLAND, such alternative mechanisms of solar neutrino conversion will still be interesting for study since their sub-leading admixture will be testable, as discussed in [37]. For example, if KamLAND confirms the LMA solution, one can place a constraint on $\mu B_\perp$, which are sensitive to how good is the KamLAND determination of the LMA oscillation parameters [41] and also to the ultimate central $\Delta m^2_{\rm SOL}$ value indicated by this experiment.

Last, but not least, solar neutrino data to derive stringent bounds on Majorana neutrino transition moments [35] when LMA-MSW oscillations account for the solar neutrino data, as discussed in ref. [42]. Should such TMs be present, they would contribute to the neutrino–electron scattering cross section and hence affect the signal observed in Super-Kamiokande. Assuming that LMA-MSW is the solution of the solar neutrino problem ref. [42] constrains neutrino TMs by using the latest global solar neutrino data. One finds that `all` elements of the TM matrix can be bounded at the same time. Moreover, ref. [42] shown how reactor data play a complementary role to the solar neutrino data. The resulting combined solar + reactor bound on TMs is $2 \times 10^{-10} \mu_B$ at the 90% C.L. The sensitivity of the upcoming Borexino experiment and is about an order of magnitude better, thanks to its lower energy.

Let me now turn to the possibility of non-standard neutrino matter interactions (NSI). These may also affect the propagation of neutrinos in a variety of astrophysical environments [43] and also provide an excellent description of present solar neutrino data. The allowed regions for the NSI mechanism of solar neutrino conversion are shown in Fig. 10. The required NSI values indicated by the solar data analysis are fully acceptable also for the atmospheric data. Such NSI description of solar data was also shown [36] to be slightly better than that of the LMA oscillation solution.

4.2. Probing NSI with Atmospheric neutrinos

FC-NSI interactions in the ν_μ -ν_τ channel without neutrino mass nor mixing have been shown to account for the zenith–angle–dependent deficit of atmospheric neutrinos observed in `contained` Super-K events [44, 45]. However such NSI explanation fails to reconcile these with Super-K and MACRO `up-going muons`, due to the lack of energy dependence intrinsic of NSI conversions. As a result, a pure NSI conversion in the atmospheric channel is ruled out at 99% C.L. [46]. Thus, unlike the case of solar neutrinos, the oscillation interpretation of atmospheric data is robust, NSI being allowed only at a sub-leading level.

The most recent global analysis of the atmospheric neutrino anomaly in terms of NSI shows that a pure NSI mechanism is now ruled out, while the standard $\nu_\mu \to \nu_\tau$ oscillations provide a remarkably good description of the anomaly [46]. The robustness of the atmospheric $\nu_\mu \to \nu_\tau$ oscillation hypothesis was shown to provide the most stringent and model-independent limits on flavour-changing (FC) and non-universal (NU) neutrino interactions, as illustrated in Fig. 11. These limits are for the

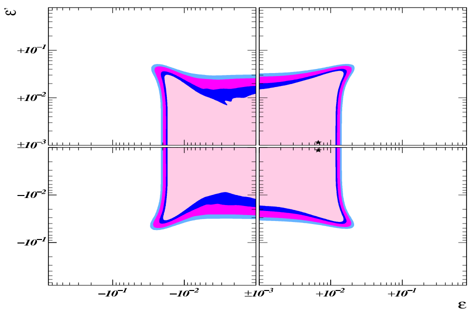

Figure 11. Atmospheric bounds on NSI, from Ref. [46].

case of NSI off-down-type quarks. They are rather model-independent, as they are obtained from pure neutrino-physics processes.

These limits are model independent as they are obtained from pure neutrino-physics processes. The stability of the neutrino oscillation solution to the atmospheric neutrino anomaly against the presence of non-standard neutrino interactions illustrates the robustness of the near-maximal atmospheric mixing and massive-neutrino hypothesis.

4.3. Probing NSI in Neutrino Factories [47, 48]

As we have seen at this conference how future neutrino factories aim at probing the lepton mixing angle θ_{13} with much better sensitivity than possible today by combining reactor and atmospheric data [46]. Given the LMA solution of the solar neutrino problem, it follows that there is a chance that indeed neutrino factories (Nufact, for short) will also probe the concurrent leptonic CP violating effects (for example, through the measurement of CP asymmetries).

The potential of such a generic Nufact in probing non-standard neutrino-matter interactions has been determined in ref. [47]. It has been found that the sensitivity to flavour-changing (FC) NSI can be substantially improved with respect to present atmospheric neutrino data, especially at energies higher than approximately 50 GeV, where the effect of the tau mass is small, as illustrated in Fig. 12. For example, a 100

GeV Nufact can probe FC neutrino interactions at the level of few $|\epsilon| <$ few $\times 10^{-4}$ at 99 % C.L.

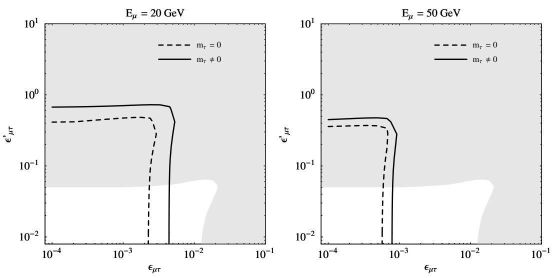

Figure 12. Nufact sensitivities to non-standard neutrino interactions, from [47].

Note also that in such hybrid solution to the neutrino anomalies, with FC-NSI explaining the solar data, and oscillations accounting for the atmospheric data, the two sectors are connected not only by the neutrino mixing angle θ_{13}, but also by the ν_e -ν_τ FC-NSI parameters. As a result NSI and oscillations may be confused, as shown in [48]. This implies that information on θ_{13} can only be obtained if bounds on NSI are available. Taking into account the existing bounds on FC interactions, one finds a drastic loss in `Nufact` sensitivities on θ_{13}, of at least two orders of magnitude. A near–detector offers the possibility to obtain stringent bounds on some NSI parameters and therefore constitutes a crucial necessary step towards the determination of θ_{13} and subsequent study of leptonic CP violation.

This work was supported by Spanish grant BFM2002-00345, by the European Commission RTN network HPRN-CT-2000-00148, by the European Science Foundation network grant N. 86.

References

[1] Proceedings of Neutrino 2002, http://neutrino2002.ph.tum.de/pages/transparencies2.html

[2] M. Maltoni, T. Schwetz, M. A. Tortola and J. W. Valle, arXiv:hep-ph/0207227 and references therein

[3] L. Wolfenstein, Phys. Rev. D **17**, 2369 (1978); S. P. Mikheev and A. Y. Smirnov, Sov. J. Nucl. Phys. **42** (1985) 913

[4] M. C. Gonzalez-Garcia, P. C. de Holanda, C. Pena-Garay and J. W. Valle, Nucl. Phys. B **573**, 3 (2000)

[5] M. C. Gonzalez-Garcia, M. Maltoni, C. Pena-Garay and J. W. Valle, Phys. Rev. D **63**, 033005 (2001)

[6] J. T. Peltoniemi, D. Tommasini and J. W. Valle, Phys. Lett. B **298**, 383 (1993). J. T. Peltoniemi and J. W. Valle, Nucl. Phys. B **406**, 409 (1993); D. O. Caldwell and R. N. Mohapatra, Phys. Rev. D **48** (1993) 325; additional references in Giunti and Lavader's excellent web–page http://www.to.infn.it/ giunti/neutrino/

[7] Talk by G. Drexlin, at Neutrino 2002

[8] M. Apollonio et al, CHOOZ Coll., Phys. Lett. B **466** (1999) 415; F. Boehm et al, Palo Verde Coll., Phys. Rev. D **64** (2001) 112001

[9] N. Fornengo, M. C. Gonzalez-Garcia and J. W. Valle, Nucl. Phys. B **580** (2000) 58 [arXiv:hep-ph/0002147].

[10] M. Maltoni, T. Schwetz and J. W. Valle, Phys. Rev. D **65**, 093004 (2002); Phys. Lett. B **518** (2001) 252

[11] S. Weinberg, Proceedings of `Neutrinos 78`, p, 1-21; R. Barbieri, J. R. Ellis and M. K. Gaillard, Phys. Lett. B **90**, 249 (1980).

[12] M. Gell-Mann, P. Ramond and R. Slansky in *Supergravity* (North Holland, Amsterdam 1979); T.

Yanagida in *Proc. of the Workshop on Unified Theory and Baryon Number of the Universe*, KEK, Japan, 1979.
[13] R. N. Mohapatra and G. Senjanovic, Phys. Rev. Lett. **44** (1980) 912; J. Schechter and J. W. Valle, Phys. Rev. D **22**, 2227 (1980); C. Wetterich, Nucl. Phys. B **187** (1981) 343.
[14] Y. Chikashige, R. N. Mohapatra and R. D. Peccei, Phys. Lett. B **98** (1981) 265; J. Schechter and J. W. Valle, Phys. Rev. D **25** (1982) 774; G. B. Gelmini and J. W. Valle, Phys. Lett. B **142**, 181 (1984).
[15] J. Schechter and J. W. Valle, Phys. Rev. D **22**, 2227 (1980); Phys. Rev. D **23**, 1666 (1981).
[16] M. Maltoni, T. Schwetz, M. A. Tortola and J. W. Valle, Nucl. Phys. B **643** (2002) 321 [arXiv:hep-ph/0207157]
[17] A. Morales, Nucl. Phys. Proc. Suppl. **77**, 335 (1999); A. Faessler and F. Simkovic, Prog. Part. Nucl. Phys. **46** (2001) 233.
[18] J. Schechter and J. W. Valle, Phys. Rev. D **25**, 2951 (1982).
[19] L. Wolfenstein, Nucl. Phys. B **186** (1981) 147. J. W. Valle and M. Singer, Phys. Rev. D **28**, 540 (1983).
[20] J. W. Valle, Phys. Rev. D **27**, 1672 (1983).
[21] V. Barger et al, Phys. Lett. B **532** (2002) 15. F. Feruglio, A. Strumia and F. Vissani, arXiv:hep-ph/0201291; H. Minakata and H. Sugiyama, Phys. Lett. B **532**, 275 (2002)
[22] Talk by Ch. Weinheimer, at Neutrino 2002
[23] O. Elgaroy et al, arXiv:astro-ph/0204152.
[24] H. V. Klapdor-Kleingrothaus et al, [GENIUS Collaboration], arXiv:hep-ph/9910205.
[25] M. Doi, T. Kotani and E. Takasugi, Prog. Theor. Phys. Suppl. **83**, 1 (1985).
[26] J. Schechter and J. W. Valle, Phys. Rev. D **21**, 309 (1980).
[27] J. W. Valle, Prog. Part. Nucl. Phys. **26**, 91 (1991).
[28] R. N. Mohapatra and J. W. F. Valle, Phys. Rev. D **34** (1986) 1642. D. Wyler and L. Wolfenstein, Nucl. Phys. B **218** (1983) 205.
[29] A. Zee, Phys. Lett. B **93** (1980) 389 [Err-ibid. B **95** (1980) 461]. K. S. Babu, Phys. Lett. B **203** (1988) 132.
[30] C. S. Aulakh and R. N. Mohapatra, Phys. Lett. B **119** (1982) 13; G. G. Ross and J. W. F. Valle, Phys. Lett. B **151** (1985) 375; J. R. Ellis et al, Phys. Lett. B **150** (1985) 142; A. Santamaria and J. W. F. Valle, Phys. Lett. B **195**, 423 (1987); Phys. Rev. Lett. **60**, 397 (1988); Phys. Rev. D **39**, 1780 (1989).
[31] L. J. Hall and M. Suzuki, Nucl. Phys. B **231** (1984) 419, see also [49] and papers therein.
[32] L. J. Hall, V. A. Kostelecky and S. Raby, Nucl. Phys. B **267** (1986) 415 R. Barbieri, L. J. Hall and A. Strumia, Nucl. Phys. B **445**, 219 (1995) F. Gabbiani et al, Nucl. Phys. B **477**, 321 (1996)
[33] J. W. Valle, Phys. Lett. B **199**, 432 (1987).
[34] E. K. Akhmedov, Phys. Lett. B **213** (1988) 64. C. S. Lim and W. J. Marciano, Phys. Rev. D **37** (1988) 1368.
[35] J. Schechter and J. W. Valle, Phys. Rev. D **24**, 1883 (1981) [Err.-ibid. D **25**, 283 (1982)].
[36] M. Guzzo et al, Nucl. Phys. B **629**, 479 (2002)
[37] J. Barranco et al, arXiv:hep-ph/0207326, Phys. Rev. D, in press
[38] O. G. Miranda et al, Phys. Lett. B **521**, 299 (2001)
[39] O. G. Miranda et al, Nucl. Phys. B **595**, 360 (2001)
[40] E. K. Akhmedov and J. Pulido, Phys. Lett. B **529**, 193 (2002)
[41] Talk by J. Shirai, at Neutrino 2002
[42] W. Grimus et al, arXiv:hep-ph/0208132. J. F. Beacom and P. Vogel, Phys. Rev. Lett. **83**, 5222 (1999)
[43] H. Nunokawa et al, Phys. Rev. D **54**, 4356 (1996); H. Nunokawa et al, Nucl. Phys. B **482**, 481 (1996); D. Grasso et al, Phys. Rev. Lett. **81**, 2412 (1998); G. L. Fogli et al, Phys. Rev. D **66**, 013009 (2002)
[44] M. C. Gonzalez-Garcia et al, Phys. Rev. Lett. **82**, 3202 (1999)
[45] N. Fornengo et al, JHEP **0007**, 006 (2000)
[46] N. Fornengo et al, Phys. Rev. D **65**, 013010 (2002)
[47] P. Huber and J. W. Valle, Phys. Lett. B **523**, 151 (2001)
[48] P. Huber, T. Schwetz and J. W. Valle, Phys. Rev. Lett. **88**, 101804 (2002) and Phys. Rev. D **66**, 013006 (2002)
[49] B. Allanach et al, arXiv:hep-ph/9906224.